

Dark-matter haloes in elliptical galaxies: lost and found

A. Dekel^{1,2,3}, F. Stoehr², G.A. Mamon², T.J. Cox⁴ & J.R. Primack³

¹Racah Institute of Physics, The Hebrew University, Jerusalem 91904, Israel

²Institut d'Astrophysique and Observatoire de Paris, 98bis Boulevard Arago, Paris 75014, France

³Department of Physics, University of California, Santa Cruz CA 95064, USA

⁴Center for Astrophysics, Harvard University, 60 Garden Street, Cambridge MA 02138, USA

According to the paradigm of cosmology, all galaxies are embedded in massive dark-matter haloes.^{1,2} This picture has been challenged by surprisingly low random stellar velocities observed in the outskirts of a few ordinary elliptical galaxies, which were interpreted as evidence for a puzzling dearth of dark matter in these galaxies.^{3,4} We show that the low velocities are in fact fully compatible with the theory of galaxy formation in dark-matter haloes. Using simulations of disc-galaxy mergers involving dark matter, stars and gas,⁵⁻⁷ we find that the stellar orbits in the outer regions of the resulting elliptical galaxies are very elongated. This is because the stars now seen away from the galaxy centre either formed near the centre, or were torn by tidal forces there, and put on outgoing trajectories. We show that these elongated orbits, together with the implied steeply falling density profile of the specific observed tracers, naturally explain the low velocities despite the massive presence of dark matter.

Introduction

Strong observational evidence suggest that the mass in the Universe is dominated by cold dark matter (DM).⁸ The common spiral galaxies are known to reside in extended DM haloes. The rotational speeds of their gas discs are observed not to decline outside the visible body,¹ unlike the expectation from Keplerian circular velocities at a radius r about a mass M , $V^2 = GM/r$. Thus, the DM mass within r is growing roughly as $M(r) \propto r$ and it dominates the gravitational potential at large radii. An extrapolation based on the typical halo density profile⁹ found in simulations of the standard Λ CDM cosmology predicts an outer “virial” radius R_{vir} that is 50-100 times larger than the characteristic stellar radius, enclosing 10-20 times more DM than luminous matter, now also indicated observationally.¹⁰ The common wisdom is that the potential wells created by the DM are crucial for seeding the formation of galaxies the way we observe them.^{2,11-13}

The common hypothesis is that elliptical galaxies originate from mergers of spirals¹⁴ and should therefore be embedded in similar DM haloes. There is evidence for DM in giant ellipticals, from X-ray¹⁵ and gravitational lensing,¹⁶ and from stellar kinematics in nearby dwarf ellipticals.¹⁷ However, ordinary ellipticals lack obvious velocity tracers at the large radii where the DM is expected to be important. This is typically beyond R_{eff} ,¹⁸ the “effective” radius encompassing half the projected light, while measurements of the projected velocity dispersion σ_p of the diffuse stellar light are limited to projected radii $r_p < 2R_{\text{eff}}$.

The strong [OIII] emission line at 5007Å from Planetary Nebulae (PN) — hot shells of gas expelled from dying stars of $(1 - 3)M_\odot$ — provide a unique tool for extracting $\sigma_p(r_p)$ beyond R_{eff} . Romanowsky et al. (R03)⁴ measured σ_p from ~ 100 bright PNs in each of three normal ellipticals, NGC 821, 3379 and 4494, adding to 531 PNs in NGC 4697 by Mendez et al. (M01).³ They find that σ_p typically drops by a factor $\simeq 1.6$ between $r_p = R_{\text{eff}}$ and $3R_{\text{eff}}$, and estimated the mass-to-light ratio within a few R_{eff} to be low, consistent with a “naked” stellar population. They interpreted this as “little if any DM in these galaxies’ haloes”, in conflict with the conventional paradigm. They noticed that anisotropic velocity dispersions could in principle produce low σ_p , but argued that their models rule out such “pathological” orbit structure. In further modeling of these and other ellipticals¹⁹ they continue to assume little or no anisotropy, and recover a similar problem. These results seem to pose a challenge to theory, and have already triggered radical explanations.²⁰

Anisotropic velocity dispersion

For given density profiles, a lower σ_p can result from more radial velocities. The dynamics implies in this case a lower 3D velocity dispersion σ because the pressure needed for balancing the gravity in hydrostatic equilibrium is provided by a radial component σ_r that corresponds to a lower σ . The projection then introduces a further decrease in σ_p . This can be illustrated by toy models made purely of circular or radial orbits, with the same constant speed and random orientations. If the stellar-density profile is steep enough, σ_p is dominated by the tangential contribution near the equatorial plane perpendicular to the line of sight, which is high for circular orbits and low for radial orbits.

The collisionless Boltzmann equation implies that the 3D profiles of any component of a spherical gravitating system in equilibrium obey the spherical Jeans equation,²¹

$$V^2(r) = [\alpha(r) + \gamma(r) - 2\beta(r)] \sigma_r^2(r) . \quad (1)$$

Here $V^2(r) = GM(r)/r$ is the circular velocity. The density profile $\nu(r)$ of the relevant stellar component enters via $\alpha \equiv -d \ln \nu / d \ln r$. Its velocity dispersion consists of radial and tangential components, $\sigma^2 = \sigma_r^2 + 2\sigma_\theta^2$; we define $\gamma \equiv -d \ln \sigma_r^2 / d \ln r$. The velocity anisotropy is $\beta \equiv 1 - \sigma_\theta^2 / \sigma_r^2$, with $\beta = -\infty, 0, 1$ for circular, isotropic and radial orbits respectively. The projection can be performed analytically when β , α and γ are constant

with r (power-law profiles, $V^2 = V_0^2 r^{-\gamma}$):

$$\sigma_p^2(r_p) = A(\alpha, \gamma) \left(\frac{(\alpha + \gamma) - (\alpha + \gamma - 1)\beta}{(\alpha + \gamma) - 2\beta} \right) V_0^2 r_p^{-\gamma} \quad (2)$$

(A in Methods). Note that σ_p is a decreasing function of β and of α . Local fits to the de-projection of the standard de Vaucouleurs²² surface-brightness profile of ellipticals give $\alpha \simeq 3.3.13-3.37$ at $2-3R_{\text{eff}}$.¹⁸ Our eyeball fits to $\sigma_p(r)$ in the observed ellipticals beyond R_{eff} yield $\gamma \simeq 0.9 \pm 0.1$. With such values we obtain $\sigma_p \simeq 0.45[(4.2 - 3.2\beta)(4.2 - 2\beta)]^{1/2} V_0 r_p^{-0.45}$. It drops by a factor ~ 1.5 between $\beta = 0$ and 1. We learn that one could match the observed low σ_p either by a low V_0 or by a high β , and that a high α helps.

In a more realistic model, we assume for the tracer stars a Sersic density profile^{23,24,18} (which reduces to de Vaucouleurs' for $m = 4$), and for the DM halo a standard density profile⁹ with a typical concentration (~ 10),²⁵ put together with a virial stellar mass fraction ~ 0.06 . With $\beta = 0$ we recover the apparent discrepancy, but when $m \simeq 4$ and $\beta \simeq 0.5$ beyond R_{eff} , the model σ_p is reduced to within $\sim 1\sigma$ of the observed σ_p . A good fit is obtained with either $m \simeq 4$ and $\beta \simeq 0.75$, or with $m \simeq 2.3$ (for which $\alpha \simeq 3.5$ near $2.5R_{\text{eff}}$) and $\beta \simeq 0.5$. The required β is higher than the $\beta \leq 0.2$ predicted for DM particles in typical haloes at a few R_{eff} ($\ll R_{\text{vir}}$),²⁶ so the PNs must not trace the DM velocities.

Merger simulations

Adopting the hypothesis that (at least some) ellipticals form by major mergers of spirals, we appeal to a suite of simulations of such events.⁵⁻⁷ The initial conditions involve two identical spirals on a parabolic orbit, each consisting of stellar and gaseous discs and a bulge, all embedded in a Λ CDM halo, constructed to match a range of typical disc galaxies. The gravitational and hydrodynamical evolution is followed using an SPH code,^{27,28} including gas cooling, star formation and feedback²⁹ (Methods).

Fig. 1 shows the stacked 3D profiles of the merged galaxies, DM versus stars, “old” and “new”. The DM density profile is slightly flatter than an isothermal sphere, $\rho \propto r^{-2}$, similar to simulated Λ CDM haloes after they have responded to the gas falling into their centres.³⁰ The robust stellar density falls off more steeply, $\rho \propto r^{-3.2}$, as in elliptical galaxies obeying the de Vaucouleurs profile near $2-3R_{\text{eff}}$. The density profile of the new stars is somewhat steeper, $\rho \propto r^{-3.5}$. We have $R_{\text{eff}} \simeq 0.015R_{\text{vir}}$, and the total-to-stellar mass ratio rises from $\simeq 2$ at $3R_{\text{eff}}$ to $\simeq 14$ at R_{vir} . The σ profiles of the DM and stars have similar slopes [as in eq. (2)], falling off roughly as $\sigma \propto r^{-0.2}$.

Our main new finding is the high anisotropy of the stellar velocities. While the DM velocities are almost isotropic ($\beta \sim 0.1$), the average stellar β grows from negative values at $r < R_{\text{eff}}$ to $\beta \sim 0.5$ at $r > R_{\text{eff}}$. In some cases β becomes higher than 0.75. Given $V(r)$ in the Jeans equation, the higher stellar α is compensated by a higher β and a lower σ .

The radial orbits arise because the halo stars emerge from near the galaxy centre. The old stars, from the progenitor central regions, reach a pericentre near the system centre of

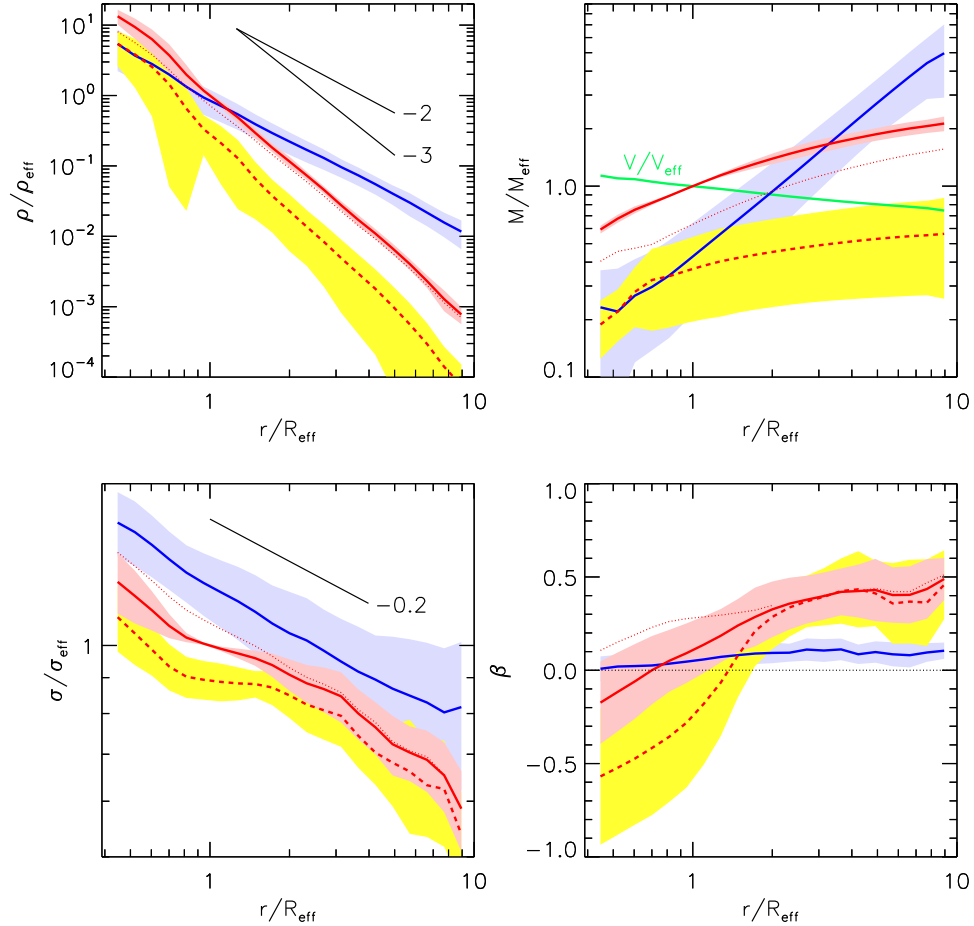


Figure 1. Three-dimensional profiles of the simulated merger remnants. Ten galaxies at two different times after the merger (typically 0.8 and 1.3 Gyr) are stacked together. Dark matter (blue) versus stars (red), divided into the old ones from the progenitors (dotted) and those newly formed during the merger (dashed). The scaling is such that the curves for the stars (all, solid red) are matched at R_{eff} . The shaded areas mark 1σ scatter. The panels refer to density ρ , mass M and circular velocity V , velocity dispersion σ and anisotropy β , with “eff” referring to the quantities at R_{eff} .

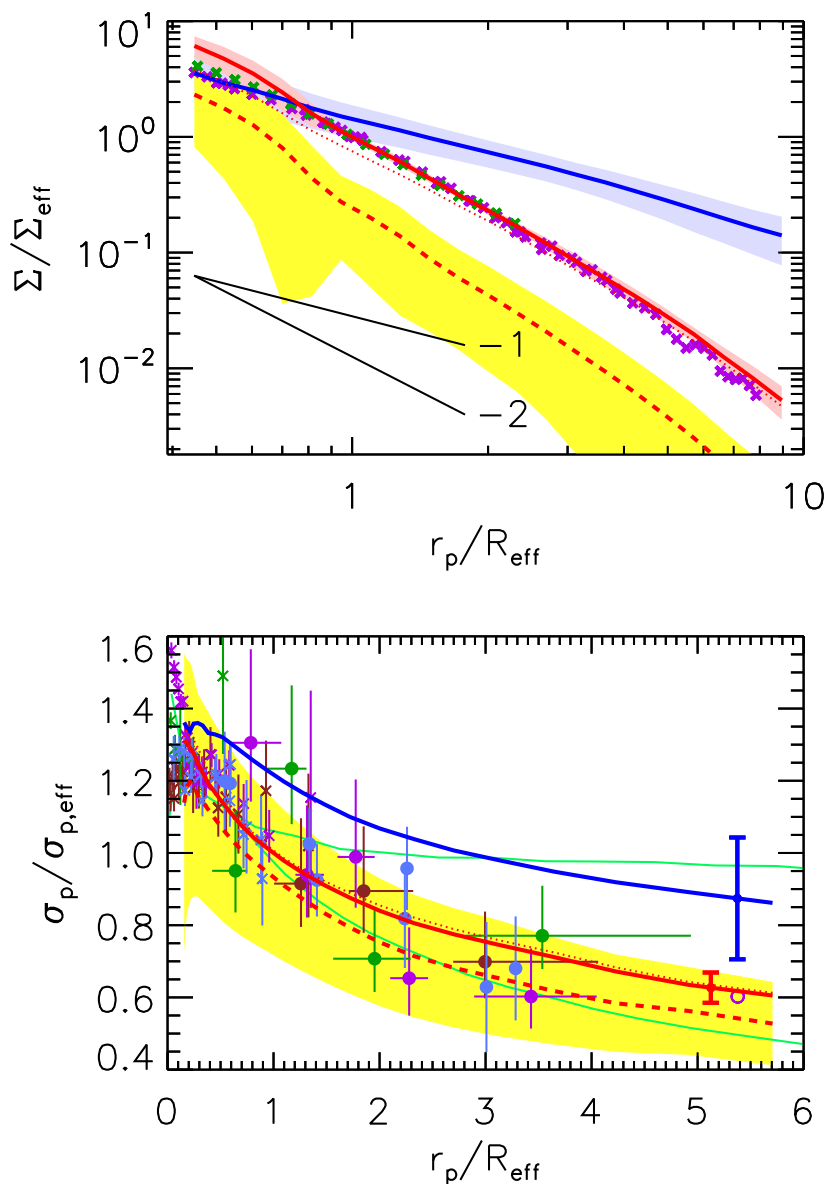


Figure 2. Projected profiles: simulated galaxies versus observations. Top: surface density. Bottom: velocity dispersion. The merger remnants are viewed from three orthogonal directions and the 60 profiles are stacked such that the stellar curves (“old” + “new”) match at R_{eff} . Dark matter (blue) versus stars (red), divided into “old” (dotted) and “new” (dashed). The < 3 Gyr “new” stars mimic the observed PNs. The shaded areas and thick bars mark 1σ scatter. The galaxies are marked green (821), violet (3379), brown (4494) and blue (4697). The surface densities shown for NGC 3379 and 4697 almost coincide with the simulated profile. Green lines refer to the R03 models with (upper) and without (lower) dark matter.

mass. The incoming and outgoing tidal streams develop a core-halo structure, with part of the stars becoming tightly bound, and the others gaining energy and flowing outward to become the halo population. The younger stars also come from the inner regions because they are produced by merger-induced gas condensations into the galaxy centres as they merge into their mutual centre.

Projected profiles

The simulated 3D profiles are projected into “observed” profiles, as viewed from three orthogonal directions, and stacked together. The data are scaled similarly (Methods). Fig. 2 shows the simulated surface-density profile and those of NGC 3379³¹ and 4697.³² They are all fit by $\Sigma \propto r_p^{-2.3}$ in the range $1-5R_{\text{eff}}$ (as in de Vaucouleurs profile at $\sim 2R_{\text{eff}}$), thus confirming the resemblance of the simulated merger remnants to typical ellipticals.

The velocity dispersions in Fig. 2 demonstrate our punchline. While the DM σ_p indeed lies above the observed points at large radii, the stellar $\sigma_p(r_p)$, $\sim 30\%$ lower, provides an acceptable match to the data. The additional $\sim 15\%$ reduction in the σ_p of the “new” stars (due to their larger α) brings the simulated profile into an excellent match with the PN data everywhere in the range $0.2-4R_{\text{eff}}$. No fiddling with model parameters is involved — simply stacking a random sample of merger remnants as simulated.

The “new” stars, 1-3 Gyr old, indeed correspond to the observed PNs. Emerging from $2-1.4M_{\odot}$ stars, their PNs are much more luminous than those of the older, less massive stars, which fall below the detection limit of M01 and R03 (Methods).

Conclusion

We conclude that the PN data is fully consistent with the standard model of galaxy formation in a Λ CDM universe, where normal ellipticals also live in massive DM haloes. The low σ_p is primarily due to the radial orbits of the halo stars, being ejected from the galaxy inner regions during the merger process. The association of the observed PNs with the younger stars formed during the merger, whose density profile is steeper, helps reducing σ_p further.

Other tracers, involving old stars, are expected to show a higher σ_p . This is especially true for globular clusters,^{33,19} which in addition tend to have a flatter density profile³⁴ and presumably a low anisotropy because of preferential tidal disruption in radial orbits. A somewhat higher σ_p is also expected in ellipticals made of gas-poor mergers involving other ellipticals, similar to the merging bulges of “old” stars in our simulations.

However, we find that even in haloes that are built by minor mergers, thus hosting spirals, the outgoing tidal tails of satellites stripped near the center bring stars into the outer halo on radial orbits. This yields a low stellar σ_p , but not as low as observed for young PNs after a merger.

We detected no significant changes between immediately after the merger and 1-2 Gyr later, but we still wish to study for how long the radial orbits persist after a long quiet

period following the last major merger. Hydrodynamical simulations of galaxy buildup via continuous mergers in a cosmological setting are the natural next step (J. Navarro et al. in preparation).

Recall⁴ that a nearly isotropic “naked” stellar system also provides a fit to the $\sigma_p(r_p)$ data inside a few R_{eff} , appealing to a low V_0 rather than a high β in eq. (2). The DM model predicts that σ_p would flatten toward $\sim 10R_{\text{eff}}$, where the “naked” model predicts a continuing decline beyond $\sim 3R_{\text{eff}}$ and very low σ_p for other tracers as well. While the “naked” model violates much of what we know about galaxy formation and cosmology, the DM model, with the radial stellar halo orbits and the steeper PN density profile, is a straightforward outcome of the self-consistent picture of structure formation in the Universe.

Methods

Equation 2

The coefficient in eq. (2) is

$$A(\alpha, \gamma) = \frac{1}{(\alpha + \gamma)} \frac{\Gamma[(\alpha + \gamma - 1)/2]}{\Gamma[(\alpha + \gamma)/2]} \frac{\Gamma[\alpha/2]}{\Gamma[(\alpha - 1)/2]}. \quad (3)$$

It is a weak function of α and γ . For instance: $A(3.5, 1.0) \simeq 0.18$, $A(3.0, 1.0) \simeq 0.20$, $A(3.5, 0.4) \simeq 0.23$, $A(3.0, 0.4) \simeq 0.26$.

Merger simulations

The merger simulations^{5–7} were designed to represent major collisions that likely occurred during the hierarchical structure formation according to the Λ CDM cosmology. The evolution is followed using the entropy-conserving, gravitating, Smoothed Particle Hydrodynamics (SPH) code GADGET.^{27,28} Gas cooling, star formation and supernova feedback are treated using simplified physical recipes²⁹ that were calibrated to match observed star-formation rates (SFR).

The progenitor disc galaxies were constructed to mimic typical big spiral galaxies, with one type (G) representing today’s typical galaxies as observed in large surveys, and another type containing more gas as in Sbc or Sc galaxies and at higher redshift. The almost-arbitrary sample analyzed here consists of four G mergers, with dark-halo masses $1.2 \times 10^{12} M_\odot$ (except one $5 \times 10^{11} M_\odot$), and five Sbc mergers plus one Sc merger with $8 \times 10^{11} M_\odot$ haloes. The baryonic fraction is $\sim 10\%$ of the DM halo mass, of which $\sim 20\%$ is gas in the G models, 50% in Sbc, and 70% in Sc. The SFR in the initial discs is regulated by supernova feedback in a quiescent mode.

Two identical galaxies are set on parabolic orbits and quickly merge because of strong dynamical friction due to their massive haloes. Our sample consists of several different orbits and orientations, including different impact parameters and prograde versus retrograde configurations. The merger typically results in two successive starbursts, one after the first close approach, and the other after the second, final coalescence. The starbursts typically occur 1-2 Gyr after the beginning of the simulation, and the remnant is “observed” ~ 1 Gyr later. The total amount of stars formed during the merger is roughly proportional to the initial gas fraction, but is not too sensitive to the orbit or orientation. The instantaneous SFR varies in the range 10-100 M_\odot/yr .

The new stars formed during the merger constitute on average $\sim 30\%$ of the total stars; typically 20% in the G cases and 40% in the Sbc cases.

The remnant galaxies resemble normal elliptical galaxies, as demonstrated above, with an ellipsoidal stellar component of a de Vaucouleurs like density profile embedded in the nearly isothermal inner region of an extended dark halo. The simulated R_{eff} involving $\sim 2 \times 10^{12} M_{\odot}$ haloes are within $\sim 20\%$ of those in three of the observed ellipticals (see below).

Scaling the data

The data from the four observed galaxies are presented together using in each case the R_{eff} determined from the surface-brightness profile.^{31,32,4} We note that the estimated R_{eff} for NGC 3379^{31,32} is $\simeq 50\%$ larger than that quoted by R03.^{4,35} In Fig. 2 we mark by an open circle the position of the last point of NGC 3379 had we used the R03 value for R_{eff} ; this uncertainty in R_{eff} does not make a qualitative difference. The amplitudes of Σ and σ_p are scaled by least-squares fits of the stellar data at $r > 0.2R_{\text{eff}}$ to the stacked simulated profile. Using as the reference a different function of a similar general shape yields similar results. The observed R_{eff} for NGC 821, 3379, 4494, 4697 match the mean simulation value after multiplication by 0.768, 1.55, 1.11, 1.15 respectively, indicating that the simulated galaxies are of comparable sizes to the observed galaxies. The corresponding σ_p were then adjusted by factors 0.885, 1.05, 0.930, 0.870 for best fit. Being close to unity, these factors indicate that the observed and simulated galaxies have a quite self-similar velocity structure.

Age of Planetary Nebulae

The luminosity of a PN in the [OIII] line is a strong increasing function of the parent stellar mass [Marigo et al. (M04),³⁶ figures 10 and 14], and hence a sharply decreasing function of its age. Once only PNs brighter than a limiting magnitude M_{5007} are detected, one can deduce an upper limit for the age t of the stellar population. The magnitude limit for the complete sample of 328 PNs in NGC 4697 by M01 is $M_{5007} \simeq -2.6$, which corresponds to $t_{M01} < 3$ Gyr (M04 figures 18, 19 or 26). With only $\simeq 100$ PNs in each of the other three galaxies by R03, their magnitude limit is brighter (by about -0.8 magnitudes based on the difference in telescope gathering area), corresponding to even younger stars. Based on the theoretical PN luminosity functions in figures 18 or 26 of M04, if the population is typically older than 1 Gyr in all four galaxies, then $t_{R03} < 2$ Gyr. We therefore adopt $t < 3$ Gyr as a conservative limit for most of the observed PNs in the four galaxies. This indicates that the PNs should be associated with the “new” stars formed during the mergers, and that the simulated mergers of discs involving gas are relevant to those ellipticals showing PNs.

Received ; Accepted .

-
1. Sofue, Y. & Rubin, V. Rotation Curves of Spiral Galaxies. *ARA&A* **39**, 137–174 (2001).
 2. White, S. D. M. & Rees, M. J. Core condensation in heavy halos - A two-stage theory for galaxy formation and clustering. *MNRAS* **183**, 341–358 (1978).
 3. Méndez, R. H., Riffeser, A., Kudritzki, R.-P., Matthias, M., Freeman, K. C., Arnaboldi, M., Capaccioli, M. & Gerhard, O. E. Detection, Photometry, and Slitless Radial Velocities of 535 Planetary Nebulae in the Flattened Elliptical Galaxy NGC 4697. *ApJ* **563**, 135–150 (2001).

4. Romanowsky, A. J., Douglas, N. G., Arnaboldi, M., Kuijken, K., Merrifield, M. R., Napolitano, N. R., Capaccioli, M. & Freeman, K. C. A Dearth of Dark Matter in Ordinary Elliptical Galaxies. *Science* **301**, 1696–1698 (2003).
5. Cox, T. J. *Simulations of Galaxy Mergers: Star Formation and Feedback*. PhD thesis UC Santa Cruz (2004). <http://physics.ucsc.edu/~tj/work/thesis/>.
6. Cox, T. J., Primack, J. R., Jonsson, P. & Somerville, R. S. Generating Hot Gas in Simulations of Disk-Galaxy Major Mergers. *ApJ* **607**, L87–L90 (2004).
7. Cox, T. J., Jonsson, P., Primack, J. R. & Somerville, R. S. The Effects of Feedback in Simulations of Disk Galaxy Major Mergers. *astro-ph/0501xxx* (2005).
8. Tegmark, M., Strauss, M. A., Blanton, M. R., Abazajian, K., Dodelson, S., Sandvik, H., Wang, X. & et al., Cosmological parameters from SDSS and WMAP. *Phys. Rev. D* **69(10)**, 103501–103527 (2004).
9. Navarro, J. F., Frenk, C. S. & White, S. D. M. A Universal Density Profile from Hierarchical Clustering. *ApJ* **490**, 493–510 (1997).
10. Prada, F., Vitvitska, M., Klypin, A., Holtzman, J. A., Schlegel, D. J., Grebel, E. K., Rix, H.-W. & et al., Observing the Dark Matter Density Profile of Isolated Galaxies. *ApJ* **598**, 260–271 (2003).
11. Fall, S. M. & Efstathiou, G. Formation and rotation of disc galaxies with haloes. *MNRAS* **193**, 189–206 (1980).
12. Blumenthal, G. R., Faber, S. M., Primack, J. R. & Rees, M. J. Formation of galaxies and large-scale structure with cold dark matter. *Nature* **311**, 517–525 (1984).
13. Dekel, A. & Silk, J. The origin of dwarf galaxies, cold dark matter, and biased galaxy formation. *ApJ* **303**, 39–55 (1986).
14. Fall, S. M. Dissipation, merging and the rotation of galaxies. *Nature* **281**, 200–202 (1979).
15. Mathews, W. G. & Brighenti, F. Hot Gas in and around Elliptical Galaxies. *ARA&A* **41**, 191–239 (2003).
16. Keeton, C. R. Cold Dark Matter and Strong Gravitational Lensing: Concord or Conflict? *ApJ* **561**, 46–60 (2001).
17. Mateo, M. L. Dwarf Galaxies of the Local Group. *ARA&A* **36**, 435–506 (1998).
18. Mamon, G. A. & Lokas, E. L. Confronting LCDM with the optical observations of elliptical galaxies: I. Is the total mass density profile of the NFW form or even steeper? *astro-ph/0405466* (2005).
19. Napolitano, N. R., Capaccioli, M., Romanowsky, A. J., Douglas, N. G., Merrifield, M. R., Kuijken, K., Arnaboldi, M. & et al., Mass-to-light ratio gradients in early-type galaxy haloes. *astro-ph/0411639* (2004).
20. Milgrom, M. & Sanders, R. H. Modified Newtonian Dynamics and the “Dearth of Dark Matter in Ordinary Elliptical Galaxies”. *ApJ* **599**, L25–L28 (2003).

21. Binney, J. & Tremaine, S. *Galactic dynamics*. Princeton, NJ, Princeton University Press (1987).
22. de Vaucouleurs, G. Recherches sur les Nebuleuses Extragalactiques. *Annales d'Astrophysique* **11**, 247–287 (1948).
23. Sersic, J. L. *Atlas de galaxias australes*. Cordoba, Argentina: Observatorio Astronomico (1968).
24. Caon, N., Capaccioli, M. & D'Onofrio, M. On the Shape of the Light Profiles of Early Type Galaxies. *MNRAS* **265**, 1013–+ (1993).
25. Bullock, J. S., Kolatt, T. S., Sigad, Y., Somerville, R. S., Kravtsov, A. V., Klypin, A. A., Primack, J. R. & Dekel, A. Profiles of dark haloes: evolution, scatter and environment. *MNRAS* **321**, 559–575 (2001).
26. Mamon, G. A. & Lokas, E. L. Confronting LCDM with the optical observations of elliptical galaxies: II. Weighing the dark matter component. astro-ph/0405491 (2005).
27. Springel, V., Yoshida, N. & White, S. D. M. GADGET: a code for collisionless and gasdynamical cosmological simulations. *New Astronomy* **6**, 79–117 (2001).
28. Springel, V. & Hernquist, L. Cosmological smoothed particle hydrodynamics simulations: the entropy equation. *MNRAS* **333**, 649–664 (2002).
29. Springel, V. Modelling star formation and feedback in simulations of interacting galaxies. *MNRAS* **312**, 859–879 (2000).
30. Gnedin, O. Y., Kravtsov, A. V., Klypin, A. A. & Nagai, D. Response of Dark Matter Halos to Condensation of Baryons: Cosmological Simulations and Improved Adiabatic Contraction Model. *ApJ* **616**, 16–26 (2004).
31. de Vaucouleurs, G. & Capaccioli, M. Luminosity distribution in galaxies. I - The elliptical galaxy NGC 3379 as a luminosity distribution standard. *ApJS* **40**, 699–731 (1979).
32. Peletier, R. F., Davies, R. L., Illingworth, G. D., Davis, L. E. & Cawson, M. CCD surface photometry of galaxies with dynamical data. II - UBR photometry of 39 elliptical galaxies. *AJ* **100**, 1091–1142 (1990).
33. Zepf, S. E., Bergond, G., Romanowsky, A. J., Rhode, K. L. & Sharples, R. M. Some Dynamical Constraints on the Halo of NGC 3379 from Wide-Field Spectroscopy of Its Globular Cluster System. *American Astronomical Society Meeting Abstracts* **205**, (2004).
34. Côté, P., McLaughlin, D. E., Hanes, D. A., Bridges, T. J., Geisler, D., Merritt, D., Hesser, J. E. & et al., Dynamics of the Globular Cluster System Associated with M87 (NGC 4486). II. Analysis. *ApJ* **559**, 828–850 (2001).
35. Burstein, D., Davies, R. L., Dressler, A., Faber, S. M., Stone, R. P. S., Lynden-Bell, D., Terlevich, R. J. & Wegner, G. Spectroscopy and photometry of elliptical galaxies. III - UBV aperture photometry, CCD photometry, and magnitude-related parameters. *ApJS* **64**, 601–642 (1987).

36. Marigo, P., Girardi, L., Weiss, A., Groenewegen, M. A. T. & Chiosi, C. Evolution of planetary nebulae. II. Population effects on the bright cut-off of the PNLF. *A&A* **423**, 995–1015 (2004).

Acknowledgments We acknowledge stimulating discussions with M. Beasley, K. Gebhardt and J. Navarro. This research has been supported by ISF 213/02 and by NASA ATP NAG5-8218. AD acknowledges a Miller Professorship at UC Berkeley, and a Blaise Pascal International Chair in Paris.

Competing interests statement The authors declare that they have no competing financial interests.

Correspondence and requests for materials should be addressed to A.D. (dekel@phys.huji.ac.il).